Salt damage risk prediction for porous limestone

H. Derluyn[1],*, P. Moonen[2], T. Diaz Gonçalves[3], V. Cnudde[1] and J. Carmeliet[4,5]

[1]Ghent University, Department of Geology and Soil Science – UGCT, Ghent, Belgium
[2]Université de Pau et des Pays de l'Adour (UPPA), Pau Cedex, France
[3]Laboratorio Nacional de Engenharia Civil (LNEC), Lisbon, Portugal
[4]ETH Zürich, Chair of Building Physics, Zürich Hönggerberg, Switzerland
[5]EMPA, Laboratory for Building Science and Technology, Dübendorf, Switzerland
* hannelore.derluyn@ugent.be

Abstract

We present a model coupling heat, moisture and salt transport, salt crystallization, deformation and damage in porous building materials with the aim of predicting crystallization-induced damage. The model performance is illustrated by simulating the damage caused by sodium chloride crystallization in a porous limestone. The results are compared with experimental observations based on neutron and X-ray imaging, showing a good agreement. The effective stresses that can cause damage are the result of the crystallization pressure combined with a sufficient amount of precipitating salt crystals in a localized zone.

Keywords: salt crystallization, salt damage, porous media, FEM modeling

1 Introduction

Many damage cases in civil constructions and in cultural heritage are related to the presence of salts. Water and dissolved salt ions penetrate into porous materials due to diffusive and convective transport. Upon changes in the environmental conditions (temperature and vapor pressure), salts can crystallize. When salt crystals form inside the material (subflorescence), crystallization pressures develop. This may lead to spalling and cracking of the building material, reducing its service life time.

The availability of a model providing a full coupling between heat, moisture and salt transport, salt crystallization, deformations and damage would be an important asset for engineers and conservators. It would allow them to assess and compare different maintenance, repair or conservation techniques or to assess the durability of a new building material under different climatic conditions, without having to perform long-term experiments. Several models for salt transport and crystallization or for damage in porous media are described in the literature. There remains however a need for bringing together the available approaches within a single unifying framework. Such a framework was only recently established, by developing a fully coupled finite element model to improve the prediction of salt damage risks in porous materials [1,2].

This paper summarizes the salt damage prediction model, and presents a case study of a hydrophobized Savonnières limestone, initially saturated with NaCl-solution, that cracks due to halite precipitation.

2 Salt damage prediction model

The model is developed in-house using the FORTRAN programming language and includes conservation of mass, energy and momentum, combined with the description of salt crystallization and crystallization damage. As this paper focuses on the salt damage prediction potential of the model, we limit this section to the description of salt crystallization and damage. For the description of the conservation laws, we refer to [2].

2.1. Salt crystallization

The salt crystal mass balance reads:

$$\Phi \frac{\partial (S_{cr}\rho_{cr})}{\partial t} = e_{crl} \tag{1}$$

with Φ the total open porosity, S_{cr} the crystal saturation degree and ρ_{cr} the crystal density. The mass exchange e_{crl} between the liquid and the crystal phase is described by the kinetics of salt crystallization or dissolution. It is

assumed that the supersaturation U is the driving force for crystallization, and that the mass exchange during crystallization is given by [3]:

$$e_{crl} = \zeta K_{m,cr}(U-1)^{g_{cr}} \quad \text{for} \quad U > U_{thr} \tag{2}$$

where $K_{m,cr}$ and g_{cr} are kinetic parameters and ζ is the fraction of the capillary active pore space filled with salt solution. In order for new crystals to nucleate and grow, the supersaturation has to exceed a threshold value U_{thr}. Dissolution is described by a similar type of equation, only the kinetic parameters differ and the threshold is $U < 1$.

For the modelling of the crystallization, besides the kinetics, also the availability of pore volume space needs to be considered. If no space is available for crystals to grow, crystallization will stop and consequently the concentration in the solution will remain higher than when the crystals could grow freely. Moreover, dissolution can only take place as long as there are crystals present. Finally, the presence of crystals at a certain location influences nucleation and growth of crystals at neighbouring locations. In order to get a stable numerical method incorporating all these constraints, the mass exchange term e_{crl} is implemented as:

$$e_{crl} = f(S_{cr},1)\cdot\zeta K_{m,cr}\left(\max(U,U_{thr})-U_{thr}\right)^{g_{cr}} + f(S_{cr},0)\cdot\zeta K_{m,diss}\left(1-\min(U,1)\right)^{g_{diss}} \tag{3}$$

where the first term represents crystal growth and the second term represents crystal dissolution. The function f accounts for the constraints related to the pore and crystal volume and is described as:

$$f(x_1,x_2) = \text{sgn}(x_2 - x_1)\cdot\left(1-\exp\left(-\left|\frac{x_1 - x_2}{HBW}\right|\right)\right) \tag{4}$$

where sgn() represents the signum function, x_1 and x_2 are values, and HBW is a (numerical) parameter controlling the gradual transition between situations in which a constraint is active or not. A very low value (HBW=0.01) is selected in order to assure that the exponential function rapidly approaches zero as the difference $|x-r|$ increases and that the function f approximates as closely as possible a step function. The function f is introduced to ensure that: (1) crystallization stops when the available pore volume is occupied by salt crystals and (2) dissolution can occur as long as there are still crystals present. As long as $S_{cr}<1$, $f(S_{cr},1)$ equals 1 and the crystallization kinetics are active. When the pore volume is filled with crystals, $S_{cr}=1$, no crystallization occurs anymore and consequently $f(S_{cr},1)$ equals 0. As long as $S_{cr}>0$, $f(S_{cr},0)$ equals -1 (where the sign indicates that the crystal mass decreases). When all crystals are dissolved and $S_{cr}=0$, the dissolution kinetics stop and $f(S_{cr},0)$ equals 0.

The function U_{thr} is defined as:

$$U_{thr} = 1+\left(U_{start} - 1\right)\cdot\exp\left(-\upsilon\bar{S}_{cr}\right) \tag{5}$$

and represents the drop of the crystallization threshold from U_{start} to 1. For primary crystallization (i.e. if no crystals are present) the supersaturation has to exceed the supersaturation value U_{start} before crystallization starts. The drop from U_{start} to 1 is related to the nucleation and growth kinetics.

These kinetics determine how long a certain supersaturation U is maintained until a sufficient amount of crystals have nucleated and/or sufficiently large crystals have grown so that new crystals start to grow at lower supersaturation levels. These phenomena are incorporated in the parameter υ and the function $\bar{S}_{cr}$. $\bar{S}_{cr}$ is a measure for the amount of crystals in the immediate neighborhood, influencing the crystallization kinetics at the location being evaluated. υ quantifies how important the presence of already formed crystals is for the crystallization threshold U_{thr}. A non-local formulation is developed for the function $\bar{S}_{cr}$:

$$\bar{S}_{cr} = \frac{\int_{\Omega} w_f S_{cr} d\Omega}{\int_{\Omega} w_f d\Omega} \tag{6}$$

with w_f a weighting function, defined as a multivariate normal distribution:

$$w_f = \frac{1}{(2\pi)^{\frac{k}{2}} l^k} \exp\left(-\frac{r^2}{2l^2}\right) \tag{7}$$

with r the distance away from the evaluated point and l the influence length. k represents the number of dimensions (1, 2 or 3). The influence length l controls the extent of the crystallization zone. The smaller its value, the more localized crystallization will be.

2.2 Crystallization damage

The solid momentum balance, in the absence of body forces, reads:

$$\nabla \cdot \boldsymbol{\sigma}_s = 0 \tag{8}$$

with $\boldsymbol{\sigma_s}$ the partial stress tensor, expressed as:

$$\boldsymbol{\sigma}_s = \boldsymbol{\sigma} - bp_s \mathbf{I} \tag{9}$$

with $\boldsymbol{\sigma}$ the effective stress tensor, b the Biot coefficient, p_s the solid pressure and $\mathbf{I}$ the second order unit tensor. p_s accounts for the mechanical effects of the constituents in the pore space on the macroscopic behavior of the porous material and is defined as [2]:

$$p_s = \int_{p_{c,ref}}^{p_c} \left(S_l + S_{cr}\right) dp_c + S_{cr}\left(p_x - p_{x,ref}\right) \tag{10}$$

with S_l and S_{cr} the liquid and crystal saturation degree, respectively, p_c the capillary pressure and p_x the crystallization pressure. The effective stress tensor is given by:

$$\boldsymbol{\sigma} = \mathbf{D}\left(\boldsymbol{\varepsilon} - \alpha \mathbf{I}\left(T - T_{ref}\right)\right) \tag{11}$$

where $\mathbf{D}$ is the 4th order elasticity tensor, $\boldsymbol{\varepsilon}$ is the second-order strain tensor, α is the thermal expansion coefficient and T the temperature.

We assume that damage occurs, i.e. that a crack develops, when the jth principal component σ_j of the effective stress tensor exceeds the material strength f_t^0 .

3 Case study

3.1 Stone properties

The total open porosity Φ of the Savonnières limestone used for the experimental study was determined by vacuum saturation and amounts 26.9%. The density of the limestone equals 1975 kg/m³. During capillary saturation, only 56% of the pore space gets filled. The capillary active porosity of untreated Savonnières limestone amounts Φ_{unt} =14.9%. The other pores are only active in the over-capillary regime. When a hydrophobic treatment is applied, the treatment deactivates a fraction of the capillary active pore space, defined by the porosity Φ_h. The capillary active pore space reduces to Φ_{unt}-Φ_h. The porosity occupied by the hydrophobic treatment Φ_h at a certain position x is found by:

$$\Phi_h(x) = \Phi_{unt} - \frac{w_{l,cap}(x)}{\rho_l} \tag{12}$$

with $w_{l,cap}(x)$ the capillary moisture content at the position x, determined from the moisture profile in the capillary saturated sample, as quantified by neutron radiography. When salt crystals are precipitating, they as well reduce the capillary active pore space. The crystals occupy a fraction of the pore space $\Phi_{cr}=\Phi \cdot S_{cr}$, with S_{cr} the crystal saturation degree. The capillary active pore space reduces to Φ_{unt}-Φ_h-Φ_{cr}.

The moisture retention curve, describing the liquid saturation degree S_l in function of capillary pressure p_c, is approximated by a sum of power functions [4]:

$$S_l(p_c) = \sum_{j=1}^{s} l_j (1+(c_j p_c)^{n_j})^{\frac{1-n_j}{n_j}} \tag{13}$$

with s the number of pore systems, l_j weight factors, and c_j and n_j model parameters. The parameters as determined by [5] are adopted. When the capillary active porosity is reduced by a hydrophobic treatment and/or the presence of salt crystals, the liquid saturation degree is reduced in a simplified way by multiplying with the factor 1-Φ_h/Φ_{unt}-Φ_{cr}/Φ_{unt}.

The liquid permeability for pure water, $K_{w,unt}$, in function of capillary pressure was determined from the moisture profiles obtained by neutron imaging during a capillary uptake test [6]. The liquid permeability for a salt solution $K_{l,unt}$ is calculated from the liquid permeability of pure water as:

$$K_{l,unt} = K_{w,unt} \frac{\eta_w}{\rho_w} \frac{\rho_l}{\eta_l} \tag{14}$$

where η is the viscosity. This relation is experimentally confirmed in [6]. When the capillary active pore space is reduced by a hydrophobic treatment and/or the presence of salt crystals, the liquid permeability is reduced, similar to the liquid saturation degree, by multiplying with the factor 1-Φ_h/Φ_{unt}-Φ_{cr}/Φ_{unt}.

The vapor permeability δ_v was measured following EN ISO 12572:2001 and can be described in function of the vapor pressure p_v as:

$$\delta_v = \delta_{v,air} \cdot \left(a + b \exp \left(c \cdot \frac{p_v}{p_{v,sat}} \right) \right) \tag{15}$$

with a, b and c parameters and $p_{v,sat}$ the saturated vapor pressure. The vapor permeability in air $\delta_{v,air}$ is given by Schirmer's equation [7]. For flow perpendicular to the bedding direction of the limestone, the parameters a, b and c amount 0.0109, 8.86·10^{-6} and 8.55, respectively.

The thermal conductivity λ was measured following EN 1946-3:1999. An average thermal conductivity of 0.99 W/mK was found for dry Savonnières limestone. To incorporate the influence of moisture, the thermal conductivity of water λ_w, multiplied with the volume fraction of water, is added to the dry thermal conductivity:

$$\lambda(S_l) = \lambda_{dry} + \lambda_w \Phi S_l \tag{16}$$

The thermal capacity $c_{p,s}$ of Savonnières limestone is estimated to be 900 J/kgK. The thermal expansion coefficient α_s was determined by measuring the thermal dilation in a dynamic mechanical analyzer during a heating-cooling cycle, an average value of 5.5 µm/mK was obtained.

The E-modulus was measured during a compression test, an average E-modulus of 13.9 GPa was found perpendicular to the bedding direction. When the stone is capillary saturated, the E-modulus perpendicular to the bedding direction reduces to 11.2 GPa. The tensile strength of dry Savonnières limestone $f_{t_{dry}}^0$ was determined from a tensile test and equals 1.8 MPa perpendicular to the bedding. In the capillary saturated state, the tensile strength reduces to 1.46 MPa. The Biot coefficient of Savonnières limestone was not measured experimentally, but estimated from literature data of a similar limestone [8]. The Biot coefficient is 0.77.

3.2   Salt properties

The supersaturation U is calculated using the Pitzer ion interaction approach as described by [9], thus accounting for the non-ideal behavior of pore solutions. The crystallization pressure p_x is expressed as [10]:

$$p_x = \frac{RT}{\overline{V}_{cr}} \ln U \tag{17}$$

with R the universal gas constant, T the absolute temperature and $\overline{V}_{cr}$ the molar volume of the crystal, being 27 cm³/mole for sodium chloride. The kinetic growth parameters $K_{m,cr}$ and g_{cr} for sodium chloride equal 0.41 kg/m³s and 1. Values of 100, 10^{-4} and 1.5 are taken for the kinetic parameters υ, l and U_{start} in the U_{thr}-function.

3.3   Drying experiment

Drying of a Savonnières limestone sample (10x10x8.5 mm³) at 45°C and 5% RH, initially saturated with a 5.8 molal sodium chloride solution, has been visualized and quantified using neutron imaging analysis [1]. The sample was prepared by applying a water and vapor tight membrane on the lateral sides (aluminum tape) in order to create a one-dimensional drying process. Drying occurred in the direction perpendicular to the bedding. A hydrophobic treatment (SILRES BS 280, Wacker) was applied on the upper 3 mm of the sample. Drying could only occur through the water repellent upper part as the bottom face was sealed. The hydrophobic treatment was intended to prevent salt efflorescence and induce in-pore crystallization. During the drying, the high spatial resolution neutron radiographs (nominal pixel size of 13.5 μm) indicated considerable deformations after about 100 minutes (Fig. 1a). These deformations represent the displacements induced by crack formation due to the crystallization of sodium chloride. The cracks resulting from the salt crystallization were characterized using X-ray micro-computed tomography. The experiment revealed that the salt crystals precipitate in the upper region of the sample, mainly in the hydrophobic zone, but below the top surface. Consequently, cracks form in this zone (Fig. 1b).
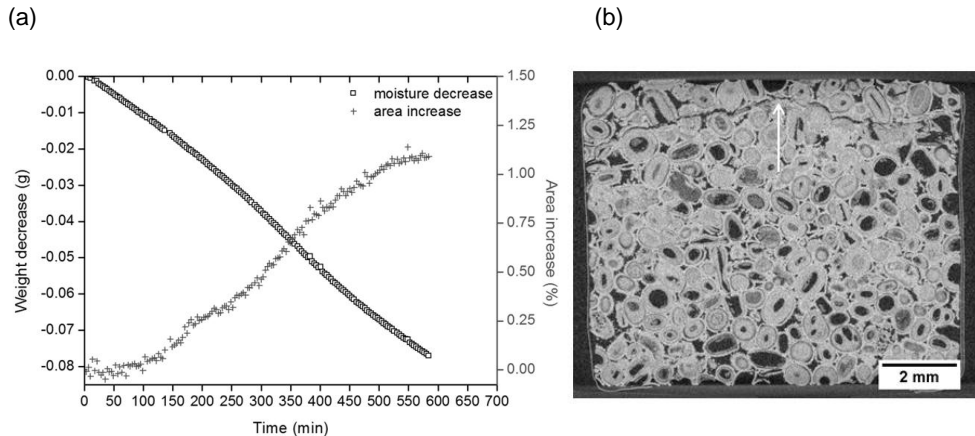
(a)   (b)

Figure 1:   (a) Weight decrease due to drying and area increase due to crystallization-induced deformations in the Savonnières sample as quantified from time-lapse neutron radiographs. After approximately 100 min. the sample starts to deform. (b) A crack, visualized by X-ray micro-tomography, is observed in the upper region of the sample after the drying process.

4   Results

We simulate the coupled heat-moisture-salt transport and salt crystallization and predict the risk for salt damage for the experiment described in section 3. The simulation is performed on a 1-dimensional mesh of length L, where L equals the height of the sample used in the drying experiment, being 8.19 mm. The mesh consists of 100 equidistant elements. The mass flux and heat flux at the sample's boundary are described by boundary conditions of the Neumann type:

$$\bar{q}_m = CMTC(p_{v,env} - p_{v,surf}) \text{ with } p_{v,env} = p_{v,sat}(T_{env}) \cdot RH_{env}$$
$$\bar{q}_e = HTC(T_{env} - T_{surf}) + \left(c_{p,v}(T_{surf} - T_0) + L_v\right) \cdot \bar{q}_m$$

(18)

$p_{v,surf}$ and T_{surf} are the vapor pressure and the temperature at the boundary surface and $p_{v,env}$, T_{env} and RH_{env} the vapor pressure, temperature and relative humidity of the environment. The convective mass transfer coefficient $CMTC$ amounts $3.95 \cdot 10^{-9}$ s/m [1] and the heat transfer coefficient HTC 5.67 W/m²K.
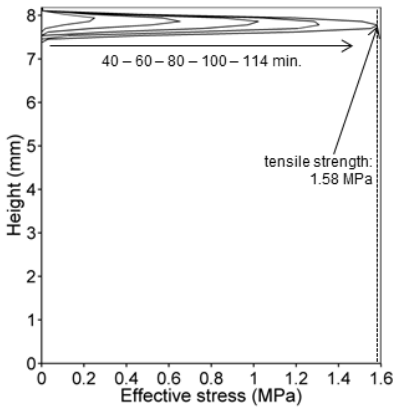

Figure 2:   Effective stress evolution.

The U_{start}-value of 1.5 is reached after 23 minutes. The effective stress evolution with time is given by the profiles in Fig. 2. We observe that the highest stresses develop at about 0.4 mm from the top of the sample. This is in agreement with the observed crack pattern in the sample (Fig. 1b). A crack developed at the same position as where the effective stress reaches the tensile strength of 1.58 MPa, (corresponding to a saturation degree of 2%). This tensile strength is reached after 114 min., similar to the time at which the deformations due to crack formation were observed in the experiment. The effective stresses are directly related to the crystal saturation degree S_{cr} and the crystallization pressure p_x (Fig. 3). It is the product of these two quantities that determines the effective stress, as expressed by equation (10). As our sample can deform freely, the solid stress σ_s equals zero (i.e. is equal to the external mechanical stress). This means that the effective stress σ is only determined by the solid pressure p_s. Using equation (10) and considering that our simulation is 1-dimensional, so that we can denote the stresses by a scalar (i.e. we describe the stress along the height of the sample), lead to:

$$\sigma = b\left(\int_0^{p_c}\left(S_{l,unt}\left(1 - \frac{\Phi_h}{\Phi_{unt}}\right)\right) dp_c + S_{cr}p_x\right)$$

The effect of the hygric stresses, expressed by the first term, is found to be negligible in this simulation, as they only range in the order of magnitude of 1000 Pa. Thus the effective stress is approximated by $\sigma \approx bS_{cr}p_x$.
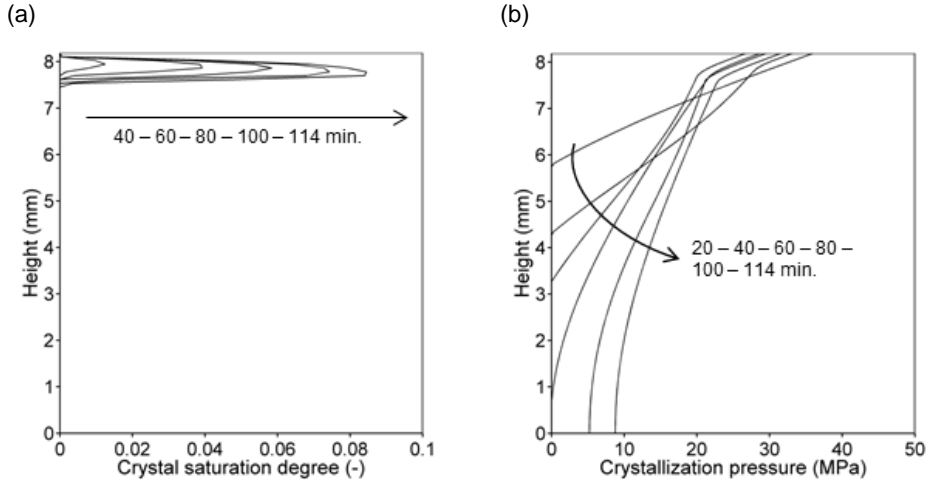
(a)   (b)

Figure 3:   Evolution of (a) the crystal saturation degree S_{cr} and (b) the crystallization pressure p_x.

5   Conclusions

We have developed a fully coupled computational model that describes heat, water and salt transport, salt crystallization and deformations and damage induced by hygro-thermal and crystallization stresses. The model predicts the macroscopic behavior and physical degradation of porous materials. The model has been discussed with the focus on the prediction of salt damage caused by the formation of sodium chloride crystals in a porous limestone during drying. The simulation results show a good agreement with experimental data, obtained from neutron and X-ray imaging techniques, when choosing adequate parameters for the crystallization kinetics. The simulations show that the effective stresses resulting from salt crystallization do not only depend on the crystallization pressure, which is related to the supersaturation, but also on the amount of salt crystals forming and the localization of these crystals.

Acknowledgements

References

[1] Derluyn, H. Salt transport and crystallization in porous limestone: neutron – X-ray imaging and poromechanical modeling, PhD Thesis, ETH Zurich, Switzerland, 2012.

[2] Derluyn, H., Moonen, P., Carmeliet, J. Deformation and damage due to drying-induced salt crystallization in porous limestone, Journal of the Mechanics and Physics of Solids (63) (2014) 242-255.

[3] Espinosa, R.M., Franke, L., Deckelmann, G. Phase changes of salts in porous materials: crystallization, hydration and deliquescence, Construction and Building Materials (22) (2008) 1758-1773.

[4] van Genuchten, M.T. A closed-form equation for predicting the hydraulic conductivity of unsaturated soils, Soil Science Society of America Journal (44) (1980) 892-898.

[5] Roels, S., Elsen, J., Carmeliet, J., Hens, H. Characterisation of pore structure by combining mercury porosimetry and micrography, Materials and Structures (34) (2001) 76-82.

[6] Derluyn, H., Griffa, M., Mannes, D., Jerjen, I., Dewanckele, J. et al. Characterizing saline uptake and salt distributions in porous limestone with neutron radiography and X-ray micro-tomography, Journal of Building Physics (36) (2013) 353-374.

[7] Ochs, F., Heidemann, W., Mullersteinhagen, H. Effective thermal conductivity of moistened insulation materials as a function of temperature, International Journal of Heat and Mass Transfer (51) (2008) 539-552.

[8] Lion, M., Skoczylas, F., Ledésert, B. Determination of the main hydraulic and poro-elastic properties of limestone from Bourgogne, France, International Journal of Rock Mechanics and Mining Sciences (41) (2004) 915-925.

[9] Steiger, M., Kiekbusch, J., Nicolai, A. An improved model incorporating Pitzer's equations for calculation of thermodynamic

properties of pore solutions implemented into an efficient program code, Construction and Building Materials (22) (2008) 1841-1850.

[10] Steiger, M. Crystal growth in porous materials – I: the crystallization pressure of large crystals, Journal of Crystal Growth (282) (2005) 455-469.